Molecular Therapy
Original Article

Lipidoid-siRNA Nanoparticle-Mediated IL-1β Gene Silencing for Systemic Arthritis Therapy in a Mouse Model

Ping Song,[1,2] Chuanxu Yang,[1,2] Jesper Skovhus Thomsen,[3] Frederik Dagnæs-Hansen,[3] Maria Jakobsen,[2] Annemarie Brüel,[3] Bent Deleuran,[3,4] and Jørgen Kjems[1,2]

[1]Interdisciplinary Nanoscience Center (iNANO), Aarhus University, 8000 Aarhus C, Denmark; [2]Department of Molecular Biology and Genetics, Aarhus University, 8000 Aarhus C, Denmark; [3]Department of Biomedicine, Aarhus University, 8000 Aarhus C, Denmark; [4]Department of Rheumatology, Aarhus University Hospital, 8000 Aarhus C, Denmark

Interleukin-1 beta (IL-1β) plays a central role in the induction of rheumatoid arthritis (RA). In the present study, we demonstrated that lipidoid-polymer hybrid nanoparticle (FS14-NP) can efficiently deliver siRNA against *IL-1β* (siIL-1β) to macrophages and effectively suppress the pathogenesis of experimental arthritis induced by collagen antibody (CAIA mice). FS14-NP/siIL-1β achieved approximately 70% and 90% gene-silencing efficiency in the RAW 264.7 cell line and intraperitoneal macrophages, respectively. Intravenous administration of FS14-NP/siRNA led to rapid accumulation of siRNA in macrophages within the arthritic joints. Furthermore, FS14-NP/siIL-1β treatment lowered the expression of pro-inflammatory cytokines in arthritic joints and dramatically attenuated ankle swelling, bone erosion, and cartilage destruction. These results demonstrate that FS14-NP/siIL-1β may represent an effective therapy for systemic arthritis and other inflammatory disorders.

INTRODUCTION

Rheumatoid arthritis (RA) is one of the most common systemic autoimmune disorders that primarily affects the joints and is characterized by hyperplasia, vascularization, and infiltration of inflammatory cells. RA can lead to systemic complications, bone destruction, and disability.[1,2] Increased secretion of pro-inflammatory cytokines by immune cells is essential for the induction and development of RA.[3,4] Among the pro-inflammatory cytokines, interleukin-1 (IL-1), tumor necrosis factor alpha (TNF-α), and interleukin-6 (IL-6) are mainly produced by macrophages and have been reported to be key regulators accelerating inflammation and stimulating the secretion of matrix-degrading enzymes such as matrix metalloproteinases (MMPs).[1,5,6] As one of the most important cytokines in RA, the IL-1 family is associated with acute and chronic inflammation. IL-1β has been identified as a therapeutic target that is overexpressed in synovial fluid at high concentrations, and it has been shown to induce bone erosion and cartilage destruction by stimulating MMP expression.[7,8]

The main strategy of RA treatments is disease-modifying antirheumatic drugs (DMARDs), which are further classified into biological DMARDs (bDMARDs) and synthetic DMARDs (sDMARDs).[9] For example, inhibition of IL-1β by antagonists has shown a great anti-inflammatory effect and can prevent recurrent bouts of the disease.[8,10,11] However, administration of these bDMARDs (mainly antagonists such as monoclonal antibodies) may provoke serious infections and acute anaphylaxis.[12,13] Also, sDMARDs, e.g., methotrexate (MTX) and leflunomide (LEF), are often associated with side effects, such as liver damage, bone marrow suppression, and systemic complications (S. Arava et al., 2013, Ann. Rhum. Dis., abstract).[14]

RNAi is an important mechanism for regulating gene expression by small RNA molecules via mRNA cleavage or translational inhibition. Small interfering RNA (siRNA), one of the most potent RNA-based gene regulators, can specifically downregulate virtually any target gene via RNAi, and this process has been used widely for treatment of a variety of diseases.[15–18] As such, the delivery of siRNAs to macrophages provides an alternative strategy for RA treatment.[19–21] However, the application of siRNAs has been hindered by a series of biological barriers, including enzymatic degradation in blood circulation, activation of the immune system, limited membrane crossing, and endosomal or lysosomal entrapment.[22] As a result, a variety of delivery systems for siRNA have been developed to protect siRNAs and overcome these barriers.[23] In the past few decades, the development of siRNA delivery methods based on peptides,[24–26] polymers,[27–29] liposomes,[30–34] and lipid-like materials[35,36] has achieved great success. However, there are still serious *in vivo* delivery issues concerning low transfection efficiency and toxicity that remain unresolved.[37–39] Recently, we have developed a novel polymer-lipidoid hybrid nanoparticle (FS14-NP) that is composed of Pluronic

Received 10 December 2018; accepted 1 May 2019;
https://doi.org/10.1016/j.ymthe.2019.05.002.

Correspondence: Chuanxu Yang, Interdisciplinary Nanoscience Center (iNANO), Aarhus University, Gustav Wieds Vej 14, 8000 Aarhus C, Denmark.
E-mail: chuanxuyang@inano.au.dk
Correspondence: Jørgen Kjems, Interdisciplinary Nanoscience Center (iNANO), Aarhus University, Gustav Wieds Vej 14, 8000 Aarhus C, Denmark.
E-mail: jk@mbg.au.dk

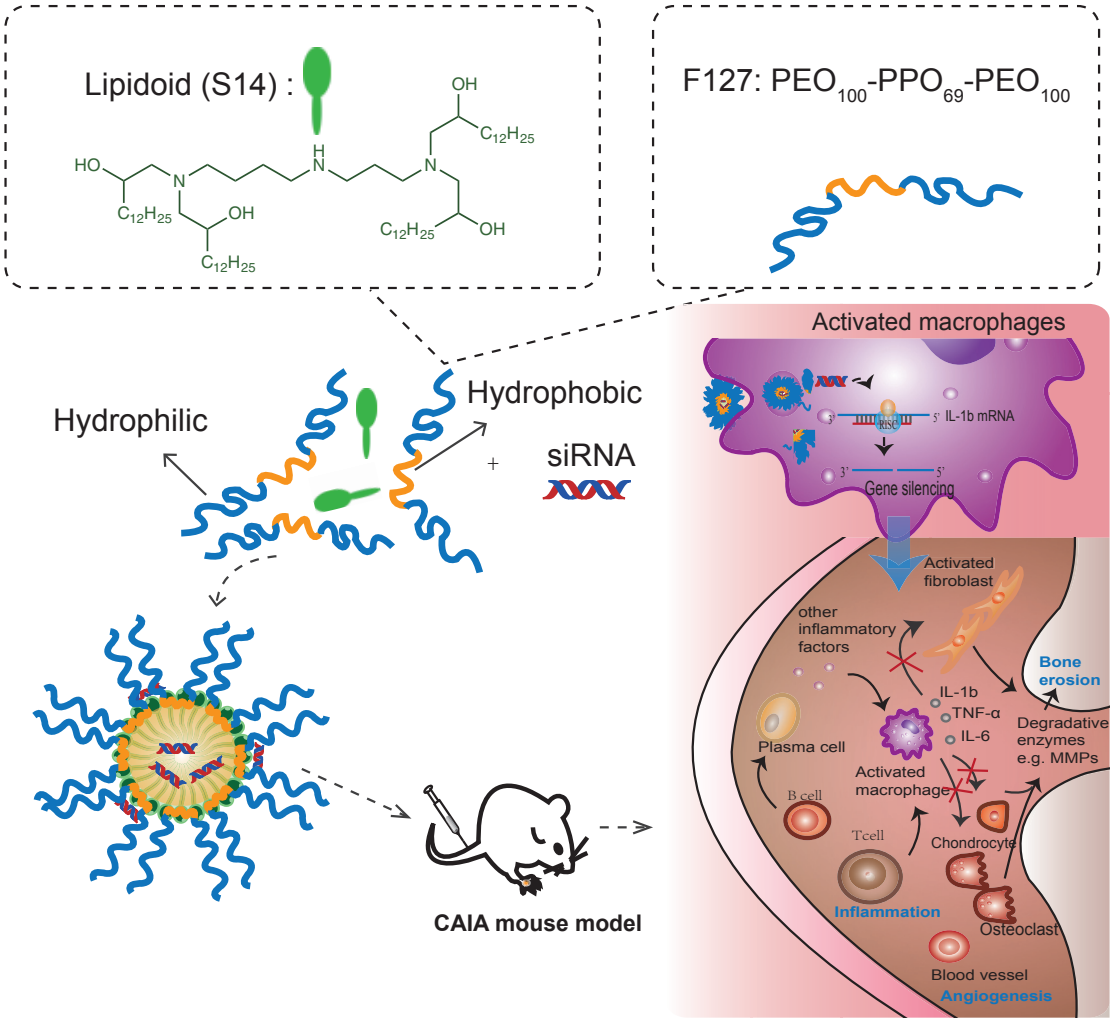

Figure 1. Schematic Illustration of the Synthesis of Lipidoid-Polymer-Based Nanoparticles and the Delivery of siRNA to CAIA Mice for Suppression of the Pathogenesis of RA

F127 and spermidine-based lipidoid (S14), which presents superior transfection efficiency in macrophages and excellent *in vivo* silencing in inflammatory models (C.Y., unpublished data).

In the present study, we evaluated the intracellular uptake and gene-silencing efficacy of siRNA against IL-1β, when delivered by polymer-lipidoid hybrid nanoparticles in both RAW 264.7 cells and intraperitoneal macrophages. We also investigated the biodistribution and therapeutic effects of FS14-NP/siIL-1β in mice with collagen-antibody-induced arthritis (CAIA).

RESULTS

Preparation and Characterization of FS14-NP

FS14-NP was synthesized by a nanoprecipitation method wherein a mixture of S14 and F127 is injected into acetate buffer. FS14-NP/siRNA complexes were further prepared through electrostatic interactions by incubating the particles with siRNAs (Figure 1). The FS14-NP measured 81.5 ± 2.07 nm in diameter with a polydispersity index (PDI) of 0.25 ± 0.01 and was positively charged at approximately +22 mV (Figure 2A, Table 1). After complexation with siRNA, the size of the FS14-NP/siRNA complex increased to 131.2 ± 3.22 nm, with a PDI of 0.34 ± 0.01. Both FS14-NP and FS14-NP/siRNA showed well-dispersed distribution and spherical shape from TEM imaging with diameters of approximately 81 and 138 nm, respectively (Figure 2B). Encapsulation efficiency was further tested, showing that FS14-NP exhibited around 80% encapsulation efficiency at a weight ratio of 5 (S14 to siRNA) without any significant change when the weight ratio was further increased to 7.5 (Figure S1A). The FS14-NP also exhibited high loading capacity (siRNA loaded:total nanoparticle weight × 100) of approximate 5.1 wt% for siRNA at the weight ratio of 5 (corresponding to an N/P ratio of 5.2).

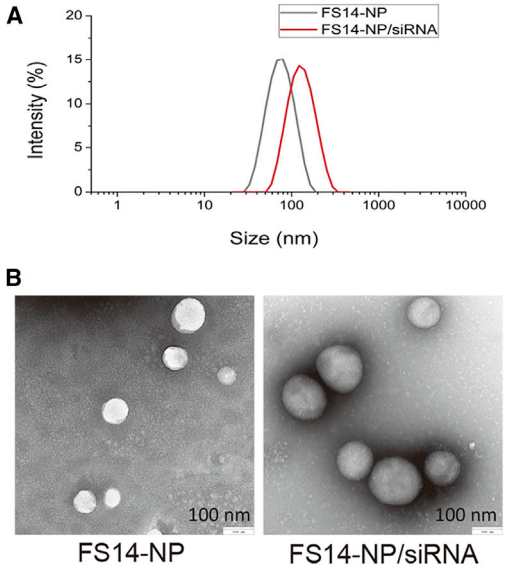

Figure 2. Characterization of FS14-NP and FS14-NP/siRNA Complex
(A) Hydrodynamic size of FS14-NP and FS14-NP/siRNA by DLS. (B) Representative TEM images of FS14-NP and FS14-NP/siRNA complexes.

In Vitro Bioactivity of FS14-NP

The *in vitro* uptake properties of FS14-NP encapsulated Cy3-labeled siRNA (FS14-NP/Cy3-siRNA) were first evaluated in the RAW 264.7 macrophage cell line treated with or without lipopolysaccharide (LPS), and compared with naked Cy3-siRNAs. Uptake of FS14-NP/Cy3-siRNA was dramatically increased upon activation of the macrophages with LPS, compared to non-activated macrophages. In contrast, there was almost no signal in activated or non-activated macrophages when treated with naked Cy3-siRNA (Figure 3A). In accordance with the confocal microscopy images, quantitative evaluation of cellular uptake for FS14-NP/Cy3-siRNA by flow cytometry showed an approximately 1.5 times higher fluorescence intensity in activated macrophages than in non-activated cells (Figure 3B). Co-staining endosomes with LysoTracker Green (green) showed only a partial overlap with Cy3-siRNAs (red) delivered by FS14-NPs after 8 h (Figure 3C), suggesting that most nanoparticles escaped the endosomes and released the siRNA into the cytoplasm.

Furthermore, the gene-silencing efficiency of FS14-NP/siIL-1β was measured on both RAW 264.7 cells and isolated primary intraperitoneal macrophages. The observed IL-1β gene-silencing efficiency of FS14-NP/siIL-1β in RAW 264.7 was over 70%, compared to 60% when using the commercial transfection reagent TKO (Mirus; Figure 3D). Even more significantly, FS14-NP/siIL-1β suppressed IL-1β expression in primary macrophages by over 95% compared with 70% for TKO/siIL-1β. Moreover, transfection with TKO seemed more toxic to the cells, as indicated by the dramatic reduction of IL-1β expression by TKO-scrambled negative control (siNC; Figure 3E). Importantly, FS14-NP/siRNA exhibited over 90% cell viability after a 24 h incubation on RAW 264.7 cells at different weight ratios (from 1.5 to 7.5; Figure S1B), confirming its high biocompatibility.

Table 1. Characterization of FS14-NP and FS14-NP/siRNA

Formulations	Size (nm)	PDI	Zeta Potential (mV)
FS14-NP	81.5 ± 2.07	0.25 ± 0.01	+21.8 ± 0.78
FS14-NP/siRNA	131.2 ± 3.22	0.34 ± 0.01	+21.4 ± 0.71

Accumulation of FS14-NP/siRNA in Arthritic Joints

To investigate the accumulation of the developed delivery system to the arthritic joints, FS14-NP encapsulated Cy5.5-labeled siRNA nanoparticles (FS14-NP/Cy5.5-siRNA) were intravenously injected into CAIA mice. Subsequently, the mice were scanned with an IVIS 200 imaging system (Xenogen, Caliper Life Sciences, Hopkinton, MA, USA) at different time points. The results demonstrated that FS14-NP/Cy5.5-siRNA exhibited much stronger signals in the inflamed joints after 4 h compared with free Cy5.5-siRNA, and the signal remained detectable for more than 24 h (Figures 4A and S2). Also, FS14-NP/Cy5.5-siRNA resulted in higher accumulation in the liver, whereas free Cy5.5-siRNA was detected only in the kidneys (Figure 4B). More importantly, paws dissected from FS14-NP/Cy5.5-siRNA-treated mice demonstrated much stronger fluorescent signals than free Cy5.5-siRNA, especially in the ankles (Figure 4C), confirming greater accumulation of FS14-NP/Cy5.5-siRNA in arthritic joints.

We also observed a great number of synovial macrophages in the vicinity of blood vessels (outlined by a white line in Figure 4D), and high levels of Cy5.5 signals (red) were found in the paw tissues from mice that received the FS14-NP/Cy5.5-siRNA treatment. In contrast, only negligible Cy5.5 signals were obtained from tissues from mice undergoing free Cy5.5-siRNA treatment. Furthermore, immunohistochemical staining showed that the majority of FS14-NP/Cy5.5-siRNA co-localized with macrophages, indicating preferential uptake into macrophages.

In Vivo Therapeutic Efficacy of FS14-NP/siRNA in CAIA Mice

Arthritis was induced in CAIA mice by intravenous injection of an antibody cocktail on day 0 and intraperitoneal injection of LPS on day 3 (CAIA mice). The CAIA mice were subsequently randomized into three groups, and PBS, FS14-NP/siIL-1β, or non-specific siRNA control particles (FS14-NP/siNC) were administered intravenously on days 2, 4, 5, and 7, respectively. Arthritis score, bodyweight loss, and ankle thickness were recorded from days 0 to 9. The results showed that FS14-NP/siIL-1β efficiently suppressed the ankle swelling and arthritis scores during arthritis progression. Representative images of hindpaws and forepaws from mice treated with FS14-NP/siIL-1β exhibited dramatic reduction in ankle swelling compared with paws from mice treated with PBS and FS14-NP/siNC on day 9 (Figure 5A). Quantification of ankle thickness and arthritis score showed significant suppression from day 5 until at least day 9 (Figures 5B and 5C). FS14-NP/siIL-1β showed approximately 73% and 52%

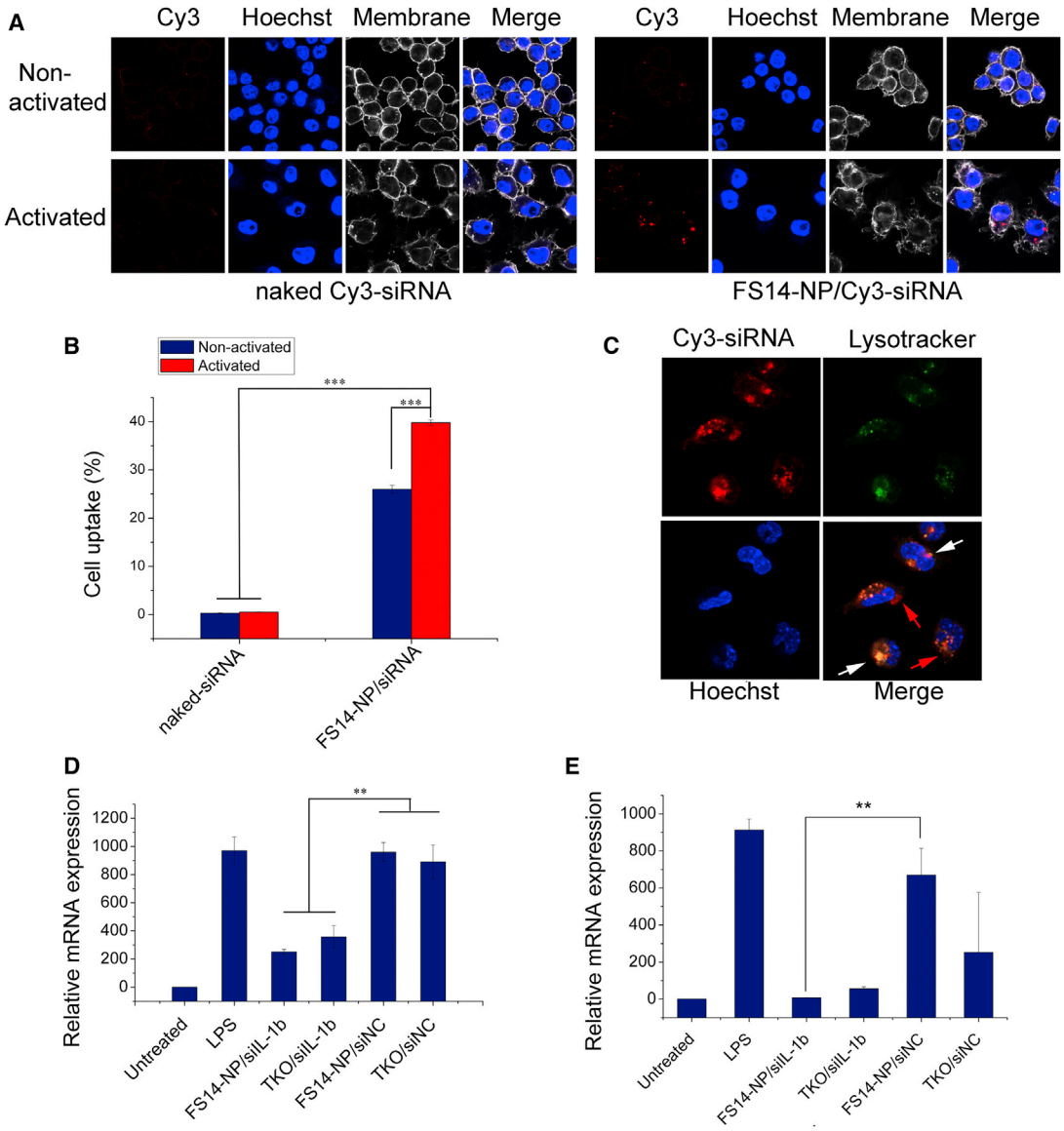

Figure 3. *In Vitro* Uptake and Gene-Silencing Effect of FS14-NP/siRNA

(A) Confocal microscopy showing cellular uptake of FS14-NP/Cy3-siRNA by both non-activated and LPS-activated RAW 264.7 cells. (B) Quantification of Cy3-labeled siRNA uptake in macrophages by flow cytometry. (C) Confocal microscopy images showing endosome escape of Cy3-siRNA (red) after an 8 h incubation with primary macrophages (red arrows indicate that siRNA escaped from the endosome into the cytoplasm; white arrows indicate some siRNA still co-localized within the endosome). (D) mRNA expression level of interleukin-1β (IL-1β) in RAW 264.7 cells and (E) primary peritoneal macrophages after transfection with FS14-NP/siIL-1β. Data are presented as means ± SD (n = 3); $^{**}p < 0.01$, $^{***}p < 0.001$.

reduction in arthritis score and ankle thickness compared to control FS14-NP/siNC on day 9. In addition, the mice receiving FS14-NP/siIL-1β (~11%) did not lose as much bodyweight as those treated with PBS (~18%) or FS14-NP/siNC (~17%) (Figure 5D). Moreover, the H&E staining of the liver from mice treated with FS14-NP/siIL-1β demonstrated less infiltration of inflammatory cells (darker cells), similar to that in untreated mice (Figure S3). Taken together, the results indicate that FS14-NP/siIL-1 induces remission of systemic inflammation without exerting adverse effects *in vivo*.

Expression of Inflammatory Cytokines in Joints

The expression of pro-inflammatory cytokines in joints was measured at both the mRNA and protein levels. In correlation with the improved clinical indexes above, FS14-NP/siIL-1β significantly reduced not only the expression of its IL-1β mRNA target, but also mRNAs for pro-inflammatory factors and matrix-degrading enzymes (IL-1β, TNF-α, MMP-3, and MMP-13) in the paws (Figures 6A and 6C–6E). No significant difference in mRNA expression was observed between administration with PBS and FS14-NP/siNC. Consolidating

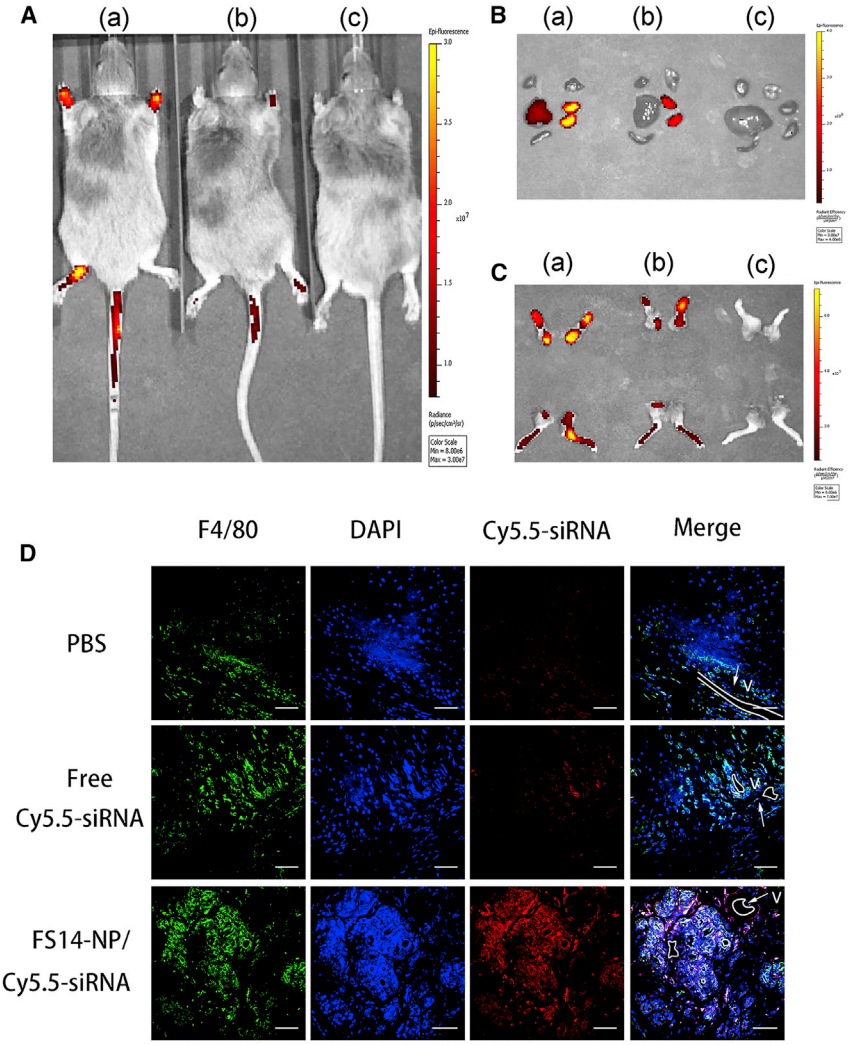

Figure 4. FS14-NP/siRNA Accumulation in Inflammatory Joints

Arthritic mice were injected intravenously with (a) FS14-NP/Cy5.5-siRNA, (b) free Cy5.5-siRNA, and (c) PBS. (A) *In vivo* imaging showing accumulation of FS14-NP/Cy5.5-siRNA in arthritic joints at 24 h after injection. (B) Organs and (C) paws were imaged after 24 h injection. (D) Co-localization of FS14-NP/Cy5.5-siRNA (red) with synovial macrophages (F4/80, green). Nuclei were stained with DAPI (blue), and blood vessels (V) are outlined (white). Scale bars, 50 μm.

this result, the suppression of IL-1β by FS14-NP/siIL-1β treatment was also observed at the protein level (Figure 6B). Moreover, the expression of IL-1β in non-targeted organs (including the liver, spleen, and kidney) showed negligible changes when treated with FS14-NP/siIL-1β, FS14-NP/siNC, or PBS (Figure S4). These results indicate that the intravenously injected FS14-NP/siIL-1β nanoparticles specifically downregulate gene expression in target tissues (joint) without adverse effect in the non-target tissues tested in our study.

Systemic Production of Pro-inflammatory Cytokines

The influence of FS14-NP/siIL-1β on systemic inflammation was further evaluated. The expression of the pro-inflammatory cytokines IL-1β, IL-6, TNF-α, and granulocyte-macrophage-colony-stimulating factor (GM-CSF) were measured in blood on day 9. As shown in Figures 7A and 7B, FS14-NP/siIL-1β significantly suppressed the systemic expression of IL-1β and -6 when compared to FS14-NP/siNC treatment, with approximately 40% and 80% reduction, respectively. Although the downregulation of IL-1β may reflect the direct silencing of the gene expression, the decline of IL-6 is probably a sign of general lowered state of inflammation in the joints. No significant difference was obtained in the expression of TNF-α (Figure S5) and the expression of GM-CSF was too low to be detected for all the treatments (data not shown).

Attenuation of Bone Destruction by Silencing of IL-1β

To assess the influence of FS14-NP/siRNA on bone destruction, the mouse legs were scanned with micro computed tomography (μCT) and dual energy X-ray absorptiometry (DEXA). 3D reconstructions of μCT scans of the paws and knees of mice receiving FS14-NP/siIL-1β treatment showed that the bone erosions did not differ significantly from those in untreated mice (normal mice) (Figure 8A). In contrast, mice treated with PBS or FS14-NP/siNC demonstrated substantial bone defects at the joints, especially in the knees, where massive erosions in the cartilage were observed (indicated by arrows). Additionally, the bone mineral content (BMC) of the paws was determined by DEXA, which is the same technique used for quantifying BMC in clinical studies. The BMC of paws from mice treated with FS14-NP/siIL-1β, PBS, or FS14-NP/siNC were, on average, 16, 14, and 13 mg, respectively. Compared to treatment with PBS or FS14-NP/siNC, treatment with FS14-NP/siIL-1β was highly effective in protecting the bone from destruction, showing a BMC similar to that in normal mice (17 mg; Figure 8B). In addition, bone erosion scores of paws from PBS, FS14-NP/siIL-1β, FS14-NP/siNC, and untreated mice were, on average, 2.33, 0.71, 1.08, and 0.25, respectively (Figure 8C). A significant difference in erosion score was found between FS14-NP/siIL-1β and PBS treatments, indicating a high proficiency of FS14-NP/siIL-1β to suppress bone erosion. However, surprisingly, no significant difference in erosion score was found between FS14-NP/siIL-1β and FS14-NP/siNC treatments.

Furthermore, the extent of inflammation and cartilage integrity was assessed by H&E and Masson-Goldner trichrome staining to evaluate

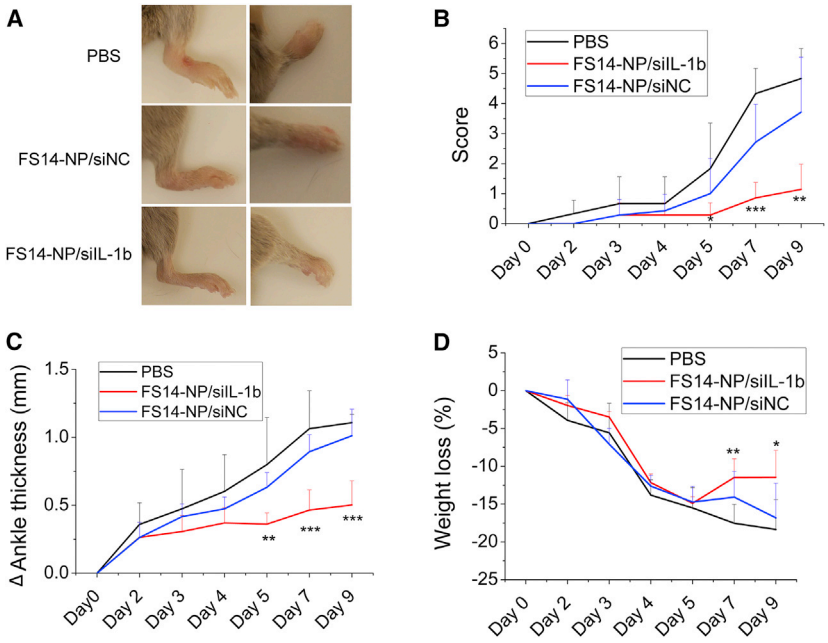

Figure 5. Therapeutic Effect of FS14-NP/siIL-1β on CAIA Mice

(A) Representative images of paws on day 9; left: hindpaw, right: forepaw. (B) Clinical scores of arthritic mice treated with PBS, FSP14/siIL-1β, or FSP14/siNC. (C) Changes in ankle thickness and (D) bodyweight loss (%) after the indicated treatment. Data are presented as means ± SD (n = 6); *p < 0.05, **p < 0.01, ***p < 0.001.

the effects of FS14-NP/siIL-1β. As shown in Figure 8D, the tissue from FS-NP/siIL-1β-treated mice appeared similar to that of untreated mice with smooth edges for collagen staining (pale pink in H&E-stained sections and blue in Masson-Goldner-trichrome-stained sections) and no sign of leukocytes influx. In contrast, the sections from PBS- and FS-NP/siNC-treated mice showed dramatic infiltration of inflammatory cells and destruction of the cartilage (red arrows).

In summary, the FS14-based delivery system demonstrated well-defined physicochemical properties; good *in vitro* biological performance, in terms of internalization and silencing efficiency; and efficient arthritis suppression *in vivo* determined by ankle swelling, expression of pro-inflammatory cytokines, and repression of bone destruction.

DISCUSSION

There have been over 50 clinical trials on the use of siRNAs for the treatment of various diseases, including diabetic, kidney injuries, tumors, and virus infections.[40] In recent years, many studies have attempted RNAi-based therapies for arthritis, which offer new possibilities in the field, in order to avoid the side effects caused by conventional DMARD treatments. Delivery of siRNAs against TNF-α is one of the most widely used therapeutic strategies for RNAi-based arthritis treatment. Chitosan- and peptide-based siRNA polyplexes have been used through both intravenous and intraperitoneal administration for the treatment of collagen-induced arthritis (CIA) mice and CAIA mice.[41–43] siRNAs against the p65 subunit of NF-κB, Notch 1, and CD40 among others, were also investigated for the treatment of arthritis.[44–46] However, siRNA-based therapies in rheumatology and delivery of siRNA against various biomarkers for arthritis demand more investigation.

IL-1β is an important marker of the severity of RA.[47] The use of antibodies against IL-1β in RA has been shown to be effective, although to a lesser degree than anti-TNF antibodies. In autoinflammatory diseases,[48] as well as in children with systemic juvenile idiopathic arthritis, anti-IL-1β is highly effective, which has led to its use in these.[49,50] Thus, the function of IL-1 inhibitory treatment is still worth studying in polyarticular arthritic conditions. In the present study, we describe a novel approach for anti-inflammatory treatment of arthritis *in vivo* by IL-1β silencing, mediated by our in-house-developed lipidoid-siRNA lipoplex. Lipidoids with hydrophobic chains of 14 carbons in length were synthesized, as they were more likely to provide high gene-silencing efficiency.[51] FS14-NP with a condensed structure was formulated through hydrophobic interactions among the lipidoid S14 and F127, in which the amphiphilic triblock copolymer F127 forms a hydrophilic corona and helps stabilize the nanoparticles in circulation. The F127 copolymer was chosen because it is widely used in pharmaceutical applications and has been approved by the U.S. Food and Drug Administration (FDA). Cellular uptake studies were conducted in both activated and non-activated macrophages, and FS14-NP was preferably internalized by activated macrophages, probably due to the natural phagocytic property of macrophages after activation.[52] This prompted us to investigate FS14-NP as a strategy for targeted delivery to macrophages in RA.

In the CAIA mouse model, arthritis is induced by a cocktail of antibodies against type II collagen, which leads to infiltration of macrophages and other inflammatory cells in the affected joints.[53] During the development of arthritis, the synovial fluid exhibits a dramatic increase in blood vessels, which are leaky, with abnormal, immature, dilated morphology.[54,55] We observed rapid accumulation of FS14-NP/siRNA to the arthritic joints (Figure 4A), which could be related to the enhanced-permeability-and-retention (EPR)-like effect of our nanoparticles.[56,57] However, the determination by immunohistochemical staining of the co-localization of FS14-NP/siRNA with macrophages (Figure 4D) indicates that the particles may be deposited into the joints primarily via infiltrating macrophages that had engulfed the particles by endocytic uptake.

Early therapeutic intervention can reduce joint damage, promote remission of inflammation, and improve the clinical outcome.[58] In

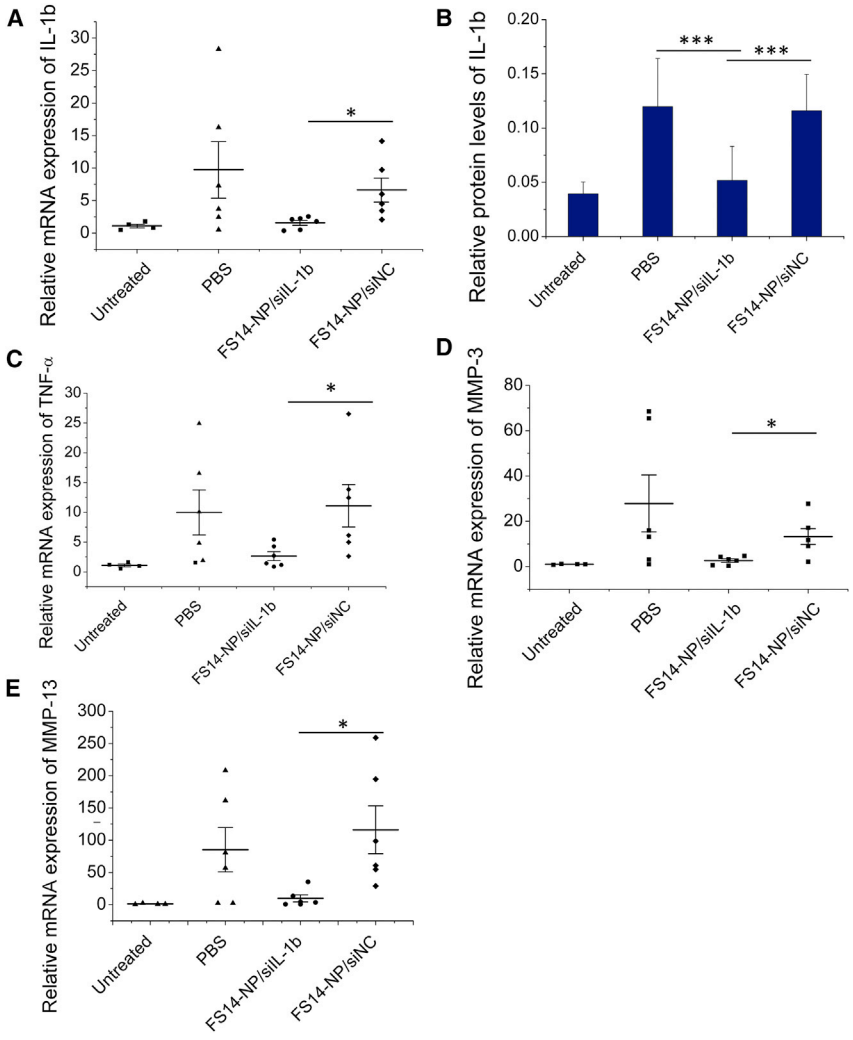

Figure 6. FS14-NP/siIL-1β Downmodulate Inflammatory Cytokines in Arthritic Joints

Paws were isolated on day 9 and homogenized. The mRNA expression for (A) IL-1β, (C) TNF-α, (D) MMP-3, and (E) MMP-13 were measured by real-time PCR, relative to GAPDH. Paw lysates were collected, and the expression of the inflammatory cytokine (B) IL-1β was assayed by ELISA; *$p < 0.05$, ***$p < 0.001$.

our study, particles were pre-administered intravenously at day 2 before LPS induction (day 3) followed by administration at days 4, 5, and 7. The therapeutic effect of FS14-NP/siIL-1β treatment was evidenced by the suppression of arthritis score, ankle thickness, and the reduction in the expression of pro-inflammatory biomarkers, such as IL-1β, TNF-α, MMP-3, and MMP-13. Specific suppression of IL-1β expression upon FS14-NP/siIL-1β delivery suggests that sequence-specific silencing of the target gene was achieved. MMPs are matrix-degrading proteinases often associated with bone and cartilage destruction, and the expression of MMPs is stimulated by IL-1β overexpression.[59] In accordance with these results, we found that expression levels of both MMP-3 and -13 were downregulated when IL-1β was silenced by FS14-NP/siIL-1β treatment (Figures 6C and 6D). In contrast, we found no evidence of IL-1β knockdown by FS14-NP/siIL-1β in other tested tissues, leaving the physiological function of other tissues largely undisturbed. Also, we found that FS14-NP/siIL-1β triggered downregulation of the pro-inflammatory cytokines IL-1β and -6 in the serum collected on day 9.

Delivery of siIL-1β by FS14-NP significantly suppressed joint destruction, indicated by a high BMC (Figure 8B) and reduced bone erosion (Figures 8A and 8C). The patellae from some of the knees in Figure 8A were missing or incomplete, which may be because of the damage sustained during dissection when isolating the bones from the muscles. Moreover, the erosion score with a trend similar to that of the arthritis score (Figures 5B, 5C, and 7C) suggests that the severity of the bone destruction is correlated with the arthritic index. Finally, the reduced influx of inflammatory cells and the preservation of cartilage integrity by FS14-NP/siIL-1β were also supported by the histological investigations.

In summary, we have demonstrated that the silencing of IL-1β by FS14-NP/siIL-1β significantly suppressed the paw swelling, expression of inflammatory cytokines, and progressive bone destruction in a mouse model of RA. Moreover, the treatment also exhibited systemic anti-inflammatory effects with reduced expression of pro-inflammatory cytokines in the circulation without affecting gene expression in non-target tissues. The results indicate that FS14-NP/siIL-1β may represent an effective therapy for arthritis and possibly also a promising treatment for other inflammatory disorders.

MATERIALS AND METHODS

Materials

Pluronic F127, spermidine, and 1,2-epoxytetradecane (ETD) were purchased from Sigma-Aldrich. IL-1β-specific siRNA (siIL-1β) and siNC were supplied by Integrated DNA Technologies (Coralville, IA, USA). IL-1β DsiRNA containing sense 5′-mAmGCmAGmCUAUGGmCAmACmUGmUUCCUGmAT-3′ and antisense 5′-UUmCAGGAAmCAmGUmUGCCAUAGCUmGCmUmUmC-3′; negative control DsiRNA containing sense 5′-mCmAUmAUmUGCGCGmUAmUAmGUmCGCGUUmAG-3′ and antisense 5′-CUmAACGCGmACmUAmUACGCGCAAUmAUmGmGmU-3′; and siEGFP with sense 5′-GACGUAAACGGCCACAAGUTC-3′ and antisense 5′-ACUUGUGG CCGUUUACGUCGC-3′were purchased from Ribotask (Denmark) and labeled at the sense strand with Cy3 or Cy5.5 for

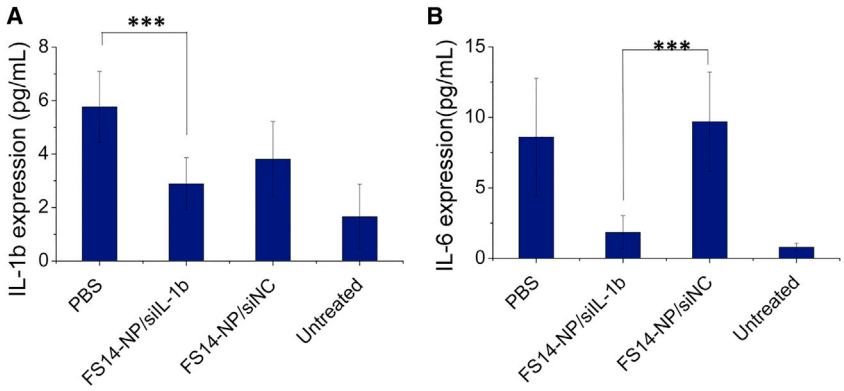

Figure 7. Systemic Expression of Inflammatory Cytokines

At day 9, blood was collected and the expression of (A) IL-1β and (B) IL-6 were measured in serum, using the Inflammatory Cytokine 4-Plex Mouse Panel kit. Data are presented as means ± SD (n = 6); ***$p < 0.001$.

bioimaging. Arthrogen-CIA arthritogenic monoclonal antibody cocktails and LPS were purchased from Chondrex (USA). Primers were all purchased from Sigma-Aldrich (Table S1).

Synthesis of Lipidoids

Lipidoids were synthesized by a ring-opening reaction between alkyl epoxides and amines (C.Y., unpublished data). In the present study, the lipidoid (S14) was synthesized between 1,2-ETD and spermidine. Briefly, spermidine and 1,2-ETD were added into a 2 mL glass vial at molar ratio of 1:4. The mixture was heated to 90°C with stirring and conducted in the dark for 2 days. Finally, the crude product was purified through chromatography on silica gel and the developing solvent from CH_2Cl_2 to the mixture of CH_2Cl_2/MeOH/NH_4OH (75:22:3) was used for gradient elution. The obtained product (S14) was a transparent, pale yellow oil that was kept at −20°C until further use.

Preparation of Nanoparticles

The lipidoid (S14) nanoparticles were formed by the nanoprecipitation method. Briefly, the synthesized lipidoid (S14) was dissolved in ethanol at a concentration of 100 mg/mL, and Pluronic F127 was dissolved in DMSO at a concentration of 100 mg/mL. Thirty microliters of the lipid-polymer mixtures (w/w, S14/F127 = 1:2) was injected quickly into 970 μL acetate buffer (200 mM, pH 5.4) with stirring, to spontaneously assemble hybrid nanoparticles (FS14-NP). FS14-NP was purified with double-distilled H_2O (ddH_2O) in a 1 kDa dialysis bag for 2 h. A centrifuge with a molecular weight cutoff (MWCO) of 10 kDa (Pall Corporation) was used for buffer exchange of the FS14-NP. To encapsulate siRNA, 20 μM of siRNA solution was mixed with FS14-NP at various weight ratios (weight of S14 to the amount of siRNA), and the mixture was incubated at 37°C for 30 min.

Characterization of FS14-NP/siRNA Nanoparticles

The size and zeta potential were determined by DLS at 25°C, with a Zetasizer Nano ZS (Malvern Instruments, Malvern, UK). The morphology was examined by transmission electron microscope (TEM; Technai G2 Spirit) operated at 120 kV. Briefly, nanoparticles were loaded on a copper grid with carbon film and stained with uranyl formate. The encapsulation efficiency for siRNA was quantified by using RiboGreen reagent (Invitrogen, Copenhagen) according to the manufacturer's instructions, and the fluorescence was measured at the excitation wavelength of 480 nm and emission wavelength of 520 nm, using a FLUOStar Optima (BMG Labtechnologies). Free siRNA was also included as a reference for the calculation of efficiency.

Cell Culture

RAW 264.7 cells (ATCC, Manassas, VA, USA) were maintained in DMEM supplemented with 10% fetal bovine serum and 1% penicillin-streptomycin at 37°C in 5% CO_2 and 100% humidity.

Primary intraperitoneal macrophages were isolated from C57BL/6J mice.[60] Briefly, 5 mL of ice-cold PBS was injected into the peritoneal cavity of the mice after sacrifice. The peritoneal fluid was collected by syringe after gentle shaking. The cells were maintained on ice before cell culture. Following isolation, the cells were grown in DMEM supplemented with 10% fetal bovine serum and 1% penicillin-streptomycin at 37°C in 5% CO_2 and 100% humidity. Finally, the non-adherent cells (non-macrophages) were washed away before further treatments.

Cell Viability

Cell viability was evaluated by AlamarBlue assay (Molecular Probes, Life Technologies) according to the manufacturer's protocol. Cells were seeded in a 96-well plate (5×10^3 cells/well) and incubated overnight. The medium was replaced with 100 μL fresh medium containing FS14-NP/siRNA at a final concentration of 50 nM siRNA at different weight ratios (S14 to siRNA) of 1.5, 3, 5, and 7.5. The cells were rinsed with PBS after a 24 h incubation and replaced with AlamarBlue reagent (10% in medium) for a 2 h incubation at 37°C. The fluorescence intensity of the supernatant (the medium) was measured by a plate reader (FLUOstar OPTIMA; Moritex BioScience) at an excitation wavelength of 540 nm and an emission wavelength of 590 nm.

Cellular Uptake Studies

Internalization of FS14-NP/Cy3-siRNA by LPS-activated macrophages was conducted in RAW 264.7 cells.[21] Briefly, the cells were seeded in 8-well tissue culture chambers at a density of 2.5×10^4 cells/well. After overnight incubation, the cells were pre-incubated with or without LPS (1 μg/mL) for 24 h, after which the medium was exchanged for fresh medium containing nanoparticles/Cy3-labeled siRNA at a final concentration of 50 nM siRNA and incubated

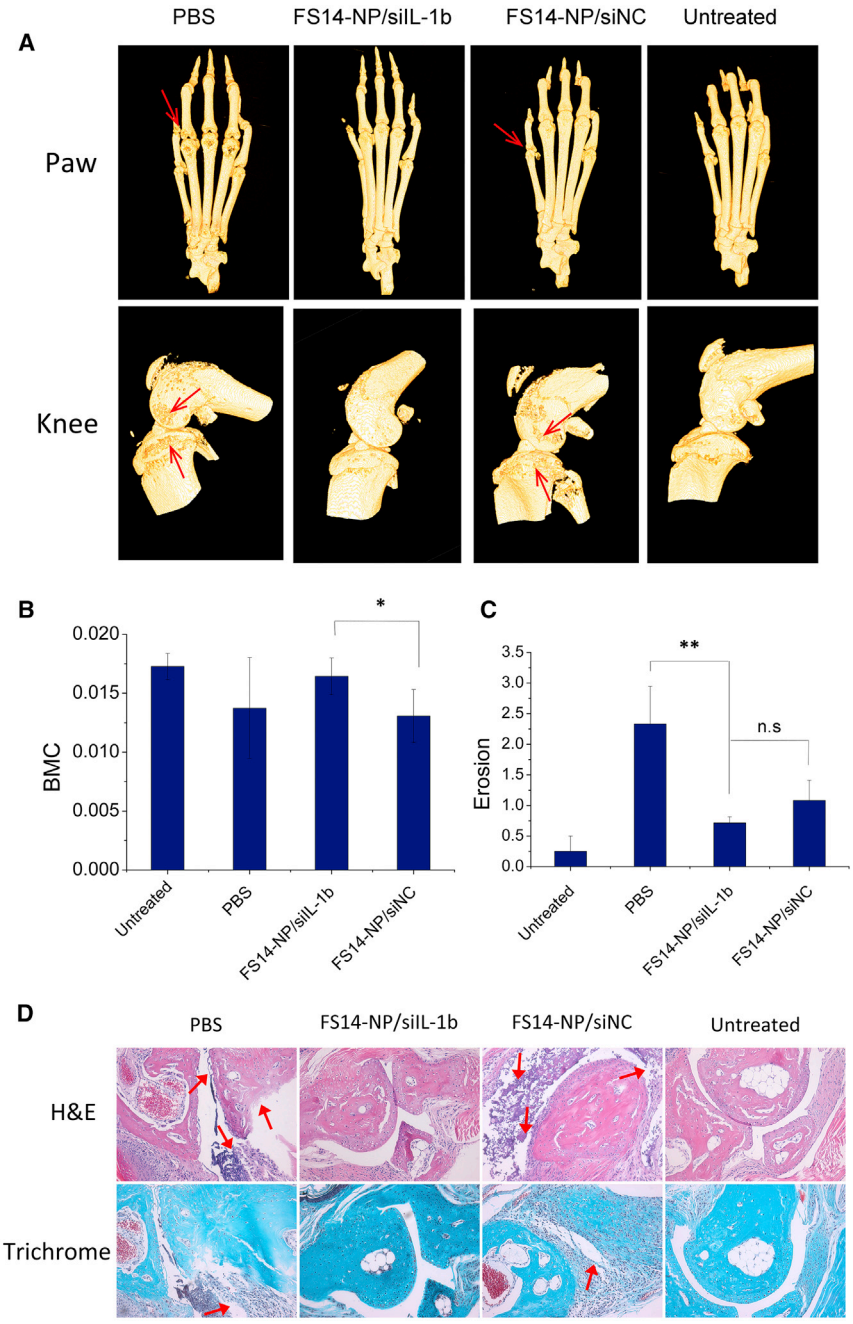

Figure 8. Bone Erosion Evaluated by μCT, DEXA, and Histology

(A) 3D reconstructed μCT images of the paws and knees from CAIA mice treated with PBS, FS14-NP/siIL-1β, or FS14-NP/siNC and untreated on day 9. (B) Bone mineral content (BMC) of paws from mice treated with PBS (14 mg), FS14-NP/siIL-1β (16 mg), or FS14-NP/siNC (13 mg) and untreated (17 mg), as determined by DEXA; means ± SD (n = 6). (C) Clinical erosion score of paws of mice treated with PBS (2.33), FS14-NP/siIL-1β (0.71), or FS14-NP/siNC (1.08) and left untreated (0.25) were evaluated in a double-blind manner: 0 represents normal joints, and 4 represents complete joint destruction. (D) Histological sections of paws stained with H&E or Masson Goldner trichrome. Influx of inflammatory cells and cartilage damage are indicated (red arrows). Means ± SEM (n = 6); *$p < 0.05$, **$p < 0.01$; NS represents no significance.

at 37°C for 1 h. After the cells were fixed with 4% paraformaldehyde, they were stained with Concanavalin A-Alexa Fluor 647 conjugate for the cell membrane and Hoechst 33342 for the nucleus (Molecular Probes). The cell uptake was visualized by confocal microscope (LSM 710; Zeiss, Germany). For the quantification of cell uptake, 5×10^4 cells/well were seeded on a 24-well plate in growth medium and incubated overnight. After pre-incubation with or without LPS (1 μg/mL) for 24 h, the medium was exchanged for fresh medium containing nanoparticles/Cy3-labeled siRNA at a final concentration of 50 nM siRNA and incubated at 37°C for 1 h. Finally, the cells were detached by 0.05% Trypsin-EDTA (Gibco, Invitrogen) and quantified by flow cytometry (Becton Dickenson).

Cellular uptake and endosome escape were further studied in primary macrophages that were seeded in 8-well tissue culture chambers (Sarstedt, Germany) at a density of 2.5×10^4 cells/well. After overnight incubation, the medium was exchanged for fresh medium containing FS14-NP/Cy3-siRNA at a final concentration of 50 nM siRNA and incubated at 37°C for 8 h. Then, the cells were incubated for 30 min with LysoTracker Green (Invitrogen), after which the cells were fixed with 4% paraformaldehyde for 10 min at room temperature and washed three times with PBS. The nucleus was then stained with Hoechst 33342 (Molecular Probes) for 10 min at 37°C. Fluorescent images were obtained with a confocal microscope (LSM 710; Zeiss, Germany).

Gene-Silencing Efficiency

The silencing efficiency was evaluated on RAW 264.7 cells and primary macrophages. Briefly, RAW 264.7 cells (5×10^4 cells/well) or primary macrophages (2×10^5 cells/well) were seeded in a 24-well plate and incubated overnight. FS14-NP/siIL-1β or FS14-NP/siNC was added to the cells at a final concentration of 50 nM and compared to the commercialized transfection reagent TKO (Mirus). After overnight incubation, the medium was replaced with 800 μL fresh medium and incubated for another 24 h. The cells were then activated with fresh medium containing 100 ng/mL LPS for 4–6 h. Gene expression was measured by quantitative PCR.

Accumulation of Lipidoid-siRNA Nanoparticles to the Inflamed Joint

The CAIA mouse model was induced with Arthrogen-CIA arthrogenic monoclonal antibody 5-clone cocktail (Chondrex). Six- to eight-week-old male DBA/1JRj (Janvier Labs, France) mice were injected intravenously with 1.5 mg/mouse of the monoclonal antibody cocktail on day 0 and injected intraperitoneally with 50 μg/mouse LPS (Chondrex) on day 3. At day 7, the mice were intravenously injected with nanoparticles containing Cy5.5-labeled scrambled siRNA or naked Cy5.5-siRNA at a dose of 0.5 mg/kg or PBS as the control. The mice were subsequently scanned after 30 min and 2, 4, and 24 h with an IVIS 200 imaging system (Xenogen, Caliper Life Sciences, Hopkinton, MA, USA) while under anesthesia with 2.5% isoflurane (IsoFlo Vet; Abbott). After 24 h, the mice were sacrificed, and the paws were harvested for immunofluorescence studies to validate the colocalization of nanoparticles with macrophages. Briefly, the paws were fixed with neutral buffered formalin for 48 h, decalcified in 10% EDTA (pH 7.4), embedded in paraffin, and sectioned at 8 μm thickness. The sections were deparaffinated and incubated with rat anti-mouse F4/80 (1:100 dilution; catalog no. 14-4801; eBioscience) and Alexa Fluor 488-conjugated AffiniPure Goat anti-rat IgG (H+L; 1:200 dilution; catalog no. 112-545-003; Jackson ImmunoResearch). Fluorescent images were taken with a confocal microscope (LSM 710; Zeiss, Germany).

Treatment of Arthritis by siRNA Delivery

Six- to eight-week-old male DBA/1JRj (Janvier Labs, France) mice were injected intravenously with 1.5 mg/mouse of the monoclonal antibody cocktail on day 0 and injected intraperitoneally with 50 μg/mouse LPS (Chondrex) on day 3. The CAIA-induced arthritic mice were intravenously injected with FS14-NP/siIL-1β or particles with an equivalent dose of random siRNA (1 mg/kg intravenously by tail vein) on days 2, 4, 5, and 7. PBS injection was used as the control. The arthritis condition was evaluated daily, with a scoring system that had a theoretical maximum of 24 points according to the requirement of the Danish Experimental Animal Inspectorate, in which 1 point was assigned for each swollen toe, 1 for tarsal and/or carpal impact, and 1 for metatarsal and/or metacarpal impact. For ethical reasons, the animals were sacrificed no later than reaching the score of 10 or 20% weight loss. The ankle thickness (two hindpaws) was determined daily with a digital calliper, and the average change in ankle thickness was calculated. Mice were weighed every second day, and the percentage of weight loss was calculated. On day 9, the mice were sacrificed, and their paws, blood, and organs were harvested for further analysis.

Evaluation of Bone Destruction

The paws were fixed in 10% buffered formalin for 48 h and washed with PBS. The BMC of the isolated paws (n = 6) was determined with a DEXA scanner (pDEXA SabreXL; Norland Stratec, Pforzheim, Germany) at a pixel size of 0.1×0.1 mm^2. In addition, the paws and knees of the mice were scanned in a μCT scanner (μCT 35; Scanco Medical, Brüttisellen, Switzerland) in high-resolution mode (1,000 projections/180°) with an isotropic voxel size of 15 μm, an X-ray tube voltage of 45 kV_p, a current of 88 μA, and an integration time of 800 ms.

The datasets of the paws and knees were visualized in 3D with Amira (version 5.6; FEI Visualization Science Group, Mérignac, France). The interactive 3D visualizations were anonymized by J.S.T., and the clinical score of the paw erosions was evaluated in a double-blind, randomized manner by P.S. and B.D., separately. The joint destruction was graded from 0 to 4, where 0 represented normal joints and 4 represented complete joint destruction.[61]

Subsequently, the paws were decalcified in EDTA, embedded in paraffin, and cut into 4-μm-thick sections. Histologic investigations including H&E and Masson-Goldner trichrome stains were carried out to further validate the inflammation and cartilage integrity.

Analysis of the Expression of Pro-inflammatory Cytokines

Paws were homogenized in PBS. After centrifugation, IL-1β and TNF-α in the supernatant were measured by ELISA (R&D Systems). Day 9 blood was drawn from the retro-orbital plexus and the concentrations of TNF-α, IL-1β, IL-6, and GM-CSF in serum were determined by using the Inflammatory Cytokine 4-Plex Mouse Panel kit (catalog no. LMC0003M; Invitrogen) according to the manufacturer's recommendation. Also, total RNA was extracted from paws, liver, spleen, and kidney with Trizol reagent (Invitrogen), according to the manufacturer's protocol. cDNA was prepared by using the Revert Aid RT Reverse Transcription Kit (catalog no. K1691) and used as the template for real-time PCR with the SYBR Green kit (Invitrogen), running on a LightCycler 480 Real-Time PCR System (Roche). The quantitative data presented are an average of mRNA expression of target gene relative to GAPDH (n = 6). Mice that were not induced were included as negative controls (untreated).

Statistics

Data are presented as means ± SD of at least three independent culture experiments, unless stated otherwise. One-way analysis of variance (ANOVA) between groups was used for statistical analysis. Statistical significance was established when $p < 0.05$.

Study Approval

The experiments were approved by the Danish Experimental Animal Inspectorate (J. no. 2014-15-0201-00001), and housing of the mice was carried out according to Danish legislation and Directive 2010/63/ on the protection of animals used for scientific purposes.

SUPPLEMENTAL INFORMATION

Supplemental Information can be found online at https://doi.org/10.1016/j.ymthe.2019.05.002.

AUTHOR CONTRIBUTIONS

P.S., C.Y., and J.S.T. performed most of the experiments. P.S. analyzed the data and wrote the manuscript. F.D.-H., M.J., A.B., and B.D. helped with various experiments. J.K. and C.Y. supervised the study. All authors read and approved the final manuscript.

CONFLICTS OF INTEREST

C.Y. is listed as inventor on a patent filed by Aarhus University concerning the use of polymer-lipid hybrid nanoparticles. The other authors declare no competing interests.

ACKNOWLEDGMENTS

This project was funded by the Lundbeck Foundation for Center for Individualized Management of Tissue Damage and Regeneration (LUNA) and Danish National Research Foundation for Center for Cellular Signal Patterns (CellPat). A postdoc grant for C.Y. was obtained from the Lundbeck Foundation (Project No. 23750). The authors also acknowledge the support of the China Scholarship Council (CSC) for P.S. The μCT scanner was donated by the VELUX Foundation. The authors also thank Anne F. Nielsen for helpful comments on the manuscript revision.

REFERENCES

1. Firestein, G.S. (2003). Evolving concepts of rheumatoid arthritis. Nature *423*, 356–361.
2. Aletaha, D., Neogi, T., Silman, A.J., Funovits, J., Felson, D.T., Bingham, C.O., 3rd, Birnbaum, N.S., Burmester, G.R., Bykerk, V.P., Cohen, M.D., et al. (2010). 2010 Rheumatoid arthritis classification criteria: an American College of Rheumatology/European League Against Rheumatism collaborative initiative. Arthritis Rheum. *62*, 2569–2581.
3. Choy, E.H.S., and Panayi, G.S. (2001). Cytokine pathways and joint inflammation in rheumatoid arthritis. N. Engl. J. Med. *344*, 907–916.
4. Brennan, F.M., and McInnes, I.B. (2008). Evidence that cytokines play a role in rheumatoid arthritis. J. Clin. Invest. *118*, 3537–3545.
5. Müller-Ladner, U., Pap, T., Gay, R.E., Neidhart, M., and Gay, S. (2005). Mechanisms of disease: the molecular and cellular basis of joint destruction in rheumatoid arthritis. Nat. Clin. Pract. Rheumatol. *1*, 102–110.
6. Feldmann, M., Brennan, F.M., and Maini, R.N. (1996). Role of cytokines in rheumatoid arthritis. Annu. Rev. Immunol. *14*, 397–440.
7. McInnes, I.B., and Schett, G. (2007). Cytokines in the pathogenesis of rheumatoid arthritis. Nat. Rev. Immunol. *7*, 429–442.
8. Dinarello, C.A. (2011). Interleukin-1 in the pathogenesis and treatment of inflammatory diseases. Blood *117*, 3720–3732.
9. Smolen, J.S., van der Heijde, D., Machold, K.P., Aletaha, D., and Landewé, R. (2014). Proposal for a new nomenclature of disease-modifying antirheumatic drugs. Ann. Rheum. Dis. *73*, 3–5.
10. Dayer, J.-M., and Bresnihan, B. (2002). Targeting interleukin-1 in the treatment of rheumatoid arthritis. Arthritis Rheum. *46*, 574–578.
11. Horai, R., Saijo, S., Tanioka, H., Nakae, S., Sudo, K., Okahara, A., Ikuse, T., Asano, M., and Iwakura, Y. (2000). Development of chronic inflammatory arthropathy resembling rheumatoid arthritis in interleukin 1 receptor antagonist-deficient mice. J. Exp. Med. *191*, 313–320.
12. Hansel, T.T., Kropshofer, H., Singer, T., Mitchell, J.A., and George, A.J.T. (2010). The safety and side effects of monoclonal antibodies. Nat. Rev. Drug Discov. *9*, 325–338.
13. Ramiro, S., Gaujoux-Viala, C., Nam, J.L., Smolen, J.S., Buch, M., Gossec, L., van der Heijde, D., Winthrop, K., and Landewé, R. (2014). Safety of synthetic and biological DMARDs: a systematic literature review informing the 2013 update of the EULAR recommendations for management of rheumatoid arthritis. Ann. Rheum. Dis. *73*, 529–535.
14. Lee, S.-M., Kim, H.J., Ha, Y.-J., Park, Y.N., Lee, S.-K., Park, Y.-B., and Yoo, K.H. (2013). Targeted chemo-photothermal treatments of rheumatoid arthritis using gold half-shell multifunctional nanoparticles. ACS Nano *7*, 50–57.
15. Kim, H.J., Kim, A., Miyata, K., and Kataoka, K. (2016). Recent progress in development of siRNA delivery vehicles for cancer therapy. Adv. Drug Deliv. Rev. *104*, 61–77.
16. Kang, J., Joo, J., Kwon, E.J., Skalak, M., Hussain, S., She, Z.-G., Ruoslahti, E., Bhatia, S.N., and Sailor, M.J. (2016). Self-Sealing Porous Silicon-Calcium Silicate Core-Shell Nanoparticles for Targeted siRNA Delivery to the Injured Brain. Adv. Mater. *28*, 7962–7969.
17. Luo, X., Wang, W., Dorkin, J.R., Veiseh, O., Chang, P.H., Abutbul-Ionita, I., Danino, D., Langer, R., Anderson, D.G., and Dong, Y. (2016). Poly(glycoamidoamine) brush nanomaterials for systemic siRNA delivery in vivo. Biomater. Sci. *5*, 38–40.
18. Wang, Y., Malcolm, D.W., and Benoit, D.S.W. (2017). Controlled and sustained delivery of siRNA/NPs from hydrogels expedites bone fracture healing. Biomaterials *139*, 127–138.
19. He, H., Zheng, N., Song, Z., Kim, K.H., Yao, C., Zhang, R., Zhang, C., Huang, Y., Uckun, F.M., Cheng, J., et al. (2016). Suppression of Hepatic Inflammation via Systemic siRNA Delivery by Membrane-Disruptive and Endosomolytic Helical Polypeptide Hybrid Nanoparticles. ACS Nano *10*, 1859–1870.
20. Kim, M.J., Park, J.-S., Lee, S.J., Jang, J., Park, J.S., Back, S.H., Bahn, G., Park, J.H., Kang, Y.M., Kim, S.H., et al. (2015). Notch1 targeting siRNA delivery nanoparticles for rheumatoid arthritis therapy. J. Control. Release *216*, 140–148.
21. Wang, Q., Jiang, H., Li, Y., Chen, W., Li, H., Peng, K., Zhang, Z., and Sun, X. (2017). Targeting NF-kB signaling with polymeric hybrid micelles that co-deliver siRNA and dexamethasone for arthritis therapy. Biomaterials *122*, 10–22.
22. Haussecker, D. (2014). Current issues of RNAi therapeutics delivery and development. J. Control. Release *195*, 49–54.
23. Whitehead, K.A., Langer, R., and Anderson, D.G. (2009). Knocking down barriers: advances in siRNA delivery. Nat. Rev. Drug Discov. *8*, 129–138.
24. Park, J.S., Yang, H.N., Jeon, S.Y., Woo, D.G., Kim, M.S., and Park, K.-H. (2012). The use of anti-COX2 siRNA coated onto PLGA nanoparticles loading dexamethasone in the treatment of rheumatoid arthritis. Biomaterials *33*, 8600–8612.
25. Moschos, S.A., Jones, S.W., Perry, M.M., Williams, A.E., Erjefalt, J.S., Turner, J.J., Barnes, P.J., Sproat, B.S., Gait, M.J., and Lindsay, M.A. (2007). Lung delivery studies using siRNA conjugated to TAT(48-60) and penetratin reveal peptide induced reduction in gene expression and induction of innate immunity. Bioconjug. Chem. *18*, 1450–1459.
26. Kim, S.W., Kim, N.Y., Choi, Y.B., Park, S.H., Yang, J.M., and Shin, S. (2010). RNA interference in vitro and in vivo using an arginine peptide/siRNA complex system. J. Control. Release *143*, 335–343.
27. Yang, C., Gao, S., Dagnæs-Hansen, F., Jakobsen, M., and Kjems, J. (2017). Impact of PEG chain length on the physical properties and bioactivity of PEGylated chitosan/siRNA nanoparticles in vitro and in vivo. ACS Appl. Mater. Interfaces *9*, 12203–12216.
28. Dong, Y., Dorkin, J.R., Wang, W., Chang, P.H., Webber, M.J., Tang, B.C., Yang, J., Abutbul-Ionita, I., Danino, D., DeRosa, F., et al. (2016). Poly(glycoamidoamine) Brushes Formulated Nanomaterials for Systemic siRNA and mRNA Delivery in Vivo. Nano Lett. *16*, 842–848.
29. Priegue, J.M., Crisan, D.N., Martínez-Costas, J., Granja, J.R., Fernandez-Trillo, F., and Montenegro, J. (2016). In Situ Functionalized Polymers for siRNA Delivery. Angew. Chem. Int. Ed. Engl. *55*, 7492–7495.
30. Jayaraman, M., Ansell, S.M., Mui, B.L., Tam, Y.K., Chen, J., Du, X., Butler, D., Eltepu, L., Matsuda, S., Narayanannair, J.K., et al. (2012). Maximizing the potency of siRNA lipid nanoparticles for hepatic gene silencing in vivo. Angew. Chem. Int. Ed. Engl. *51*, 8529–8533.
31. Semple, S.C., Akinc, A., Chen, J., Sandhu, A.P., Mui, B.L., Cho, C.K., Sah, D.W., Stebbing, D., Crosley, E.J., Yaworski, E., et al. (2010). Rational design of cationic lipids for siRNA delivery. Nat. Biotechnol. *28*, 172–176.
32. Wilson, D.S., Dalmasso, G., Wang, L., Sitaraman, S.V., Merlin, D., and Murthy, N. (2010). Orally delivered thioketal nanoparticles loaded with TNF-α-siRNA target inflammation and inhibit gene expression in the intestines. Nat. Mater. *9*, 923–928.
33. Jensen, D.K., Jensen, L.B., Koocheki, S., Bengtson, L., Cun, D., Nielsen, H.M., and Foged, C. (2012). Design of an inhalable dry powder formulation of DOTAP-modified PLGA nanoparticles loaded with siRNA. J. Control. Release *157*, 141–148.
34. Yang, C., Gao, S., Song, P., Dagnæs-Hansen, F., Jakobsen, M., and Kjems, J. (2018). Theranostic Niosomes for Efficient siRNA/MicroRNA Delivery and Activatable

Near-Infrared Fluorescent Tracking of Stem Cells. ACS Appl. Mater. Interfaces *10*, 19494–19503.

35. Wang, M., Alberti, K., Sun, S., Arellano, C.L., and Xu, Q. (2014). Combinatorially designed lipid-like nanoparticles for intracellular delivery of cytotoxic protein for cancer therapy. Angew. Chem. Int. Ed. Engl. *53*, 2893–2898.
36. Akinc, A., Zumbuehl, A., Goldberg, M., Leshchiner, E.S., Busini, V., Hossain, N., Bacallado, S.A., Nguyen, D.N., Fuller, J., Alvarez, R., et al. (2008). A combinatorial library of lipid-like materials for delivery of RNAi therapeutics. Nat. Biotechnol. *26*, 561–569.
37. Lv, H., Zhang, S., Wang, B., Cui, S., and Yan, J. (2006). Toxicity of cationic lipids and cationic polymers in gene delivery. J. Control. Release *114*, 100–109.
38. Breunig, M., Lungwitz, U., Liebl, R., and Goepferich, A. (2007). Breaking up the correlation between efficacy and toxicity for nonviral gene delivery. Proc. Natl. Acad. Sci. USA *104*, 14454–14459.
39. Majzoub, R.N., Chan, C.-L., Ewert, K.K., Silva, B.F.B., Liang, K.S., Jacovetty, E.L., Carragher, B., Potter, C.S., and Safinya, C.R. (2014). Uptake and transfection efficiency of PEGylated cationic liposome-DNA complexes with and without RGD-tagging. Biomaterials *35*, 4996–5005.
40. Ozcan, G., Ozpolat, B., Coleman, R.L., Sood, A.K., and Lopez-Berestein, G. (2015). Preclinical and clinical development of siRNA-based therapeutics. Adv. Drug Deliv. Rev. *87*, 108–119.
41. Lee, S.J., Lee, A., Hwang, S.R., Park, J.-S., Jang, J., Huh, M.S., Jo, D.G., Yoon, S.Y., Byun, Y., Kim, S.H., et al. (2014). TNF-α gene silencing using polymerized siRNA/thiolated glycol chitosan nanoparticles for rheumatoid arthritis. Mol. Ther. *22*, 397–408.
42. Ye, C., Bhan, A.K., Deshpande, V., Shankar, P., and Manjunath, N. (2013). Silencing TNF-α in macrophages and dendritic cells for arthritis treatment. Scand. J. Rheumatol. *42*, 266–269.
43. Howard, K.A., Paludan, S.R., Behlke, M.A., Besenbacher, F., Deleuran, B., and Kjems, J. (2009). Chitosan/siRNA nanoparticle-mediated TNF-α knockdown in peritoneal macrophages for anti-inflammatory treatment in a murine arthritis model. Mol. Ther. *17*, 162–168.
44. Park, J.-S., Kim, S.-H., Kim, K., Jin, C.-H., Choi, K.Y., Jang, J., Choi, Y., Gwon, A.R., Baik, S.H., Yun, U.J., et al. (2015). Inhibition of notch signalling ameliorates experimental inflammatory arthritis. Ann. Rheum. Dis. *74*, 267–274.
45. Zhou, H.F., Yan, H., Pan, H., Hou, K.K., Akk, A., Springer, L.E., Hu, Y., Allen, J.S., Wickline, S.A., and Pham, C.T. (2014). Peptide-siRNA nanocomplexes targeting NF-κB subunit p65 suppress nascent experimental arthritis. J. Clin. Invest. *124*, 4363–4374.
46. Apparailly, F., and Jorgensen, C. (2013). siRNA-based therapeutic approaches for rheumatic diseases. Nat. Rev. Rheumatol. *9*, 56–62.
47. Buchs, N., di Giovine, F.S., Silvestri, T., Vannier, E., Duff, G.W., and Miossec, P. (2001). IL-1B and IL-1Ra gene polymorphisms and disease severity in rheumatoid arthritis: interaction with their plasma levels. Genes Immun. *2*, 222–228.
48. Gabay, C., Lamacchia, C., and Palmer, G. (2010). IL-1 pathways in inflammation and human diseases. Nat. Rev. Rheumatol. *6*, 232–241.
49. Alten, R., Gomez-Reino, J., Durez, P., Beaulieu, A., Sebba, A., Krammer, G., Preiss, R., Arulmani, U., Widmer, A., Gitton, X., and Kellner, H. (2011). Efficacy and safety of the human anti-IL-1β monoclonal antibody canakinumab in rheumatoid arthritis: results of a 12-week, Phase II, dose-finding study. BMC Musculoskelet. Disord. *12*, 153.
50. Ruperto, N., Brunner, H.I., Quartier, P., Constantin, T., Wulffraat, N., Horneff, G., Brik, R., McCann, L., Kasapcopur, O., Rutkowska-Sak, L., et al.; PRINTO; PRCSG (2012). Two randomized trials of canakinumab in systemic juvenile idiopathic arthritis. N. Engl. J. Med. *367*, 2396–2406.
51. Love, K.T., Mahon, K.P., Levins, C.G., Whitehead, K.A., Querbes, W., Dorkin, J.R., Qin, J., Cantley, W., Qin, L.L., Racie, T., et al. (2010). Lipid-like materials for low-dose, in vivo gene silencing. Proc. Natl. Acad. Sci. USA *107*, 1864–1869.
52. Aderem, A., and Underhill, D.M. (1999). Mechanisms of Phagocytosis in Macrophages. Annu. Rev. Immunol. *17*, 593–623.
53. Asquith, D.L., Miller, A.M., McInnes, I.B., and Liew, F.Y. (2009). Animal models of rheumatoid arthritis. Eur. J. Immunol. *39*, 2040–2044.
54. Paleolog, E.M. (2002). Angiogenesis in rheumatoid arthritis. Arthritis Res. *4* (*Suppl 3*), S81–S90.
55. Marrelli, A., Cipriani, P., Liakouli, V., Carubbi, F., Perricone, C., Perricone, R., and Giacomelli, R. (2011). Angiogenesis in rheumatoid arthritis: a disease specific process or a common response to chronic inflammation? Autoimmun. Rev. *10*, 595–598.
56. Boyd, B.J., Galle, A., Daglas, M., Rosenfeld, J.V., and Medcalf, R. (2015). Traumatic brain injury opens blood-brain barrier to stealth liposomes via an enhanced permeability and retention (EPR)-like effect. J. Drug Target. *23*, 847–853.
57. Crielaard, B.J., Lammers, T., Schiffelers, R.M., and Storm, G. (2012). Drug targeting systems for inflammatory disease: one for all, all for one. J. Control. Release *161*, 225–234.
58. Gremese, E., Salaffi, F., Bosello, S.L., Ciapetti, A., Bobbio-Pallavicini, F., Caporali, R., and Ferraccioli, G. (2013). Very early rheumatoid arthritis as a predictor of remission: a multicentre real life prospective study. Ann. Rheum. Dis. *72*, 858–862.
59. Mengshol, J.A., Vincenti, M.P., and Brinckerhoff, C.E. (2001). IL-1 induces collagenase-3 (MMP-13) promoter activity in stably transfected chondrocytic cells: requirement for Runx-2 and activation by p38 MAPK and JNK pathways. Nucleic Acids Res. *29*, 4361–4372.
60. Davies, J.Q., and Gordon, S. (2005). Isolation and Culture of Murine Macrophages. Methods Mol Biol. *290*, 91–103.
61. Fatima, F., Fei, Y., Ali, A., Mohammad, M., Erlandsson, M.C., Bokarewa, M.I., Nawaz, M., Valadi, H., Na, M., and Jin, T. (2017). Radiological features of experimental staphylococcal septic arthritis by micro computed tomography scan. PLoS ONE *12*, e0171222.

YMTHE, Volume *27*

Supplemental Information

Lipidoid-siRNA Nanoparticle-Mediated IL-1β Gene Silencing for Systemic Arthritis Therapy in a Mouse Model

Ping Song, Chuanxu Yang, Jesper Skovhus Thomsen, Frederik Dagnæs-Hansen, Maria Jakobsen, Annemarie Brüel, Bent Deleuran, and Jørgen Kjems

Supplemental Information

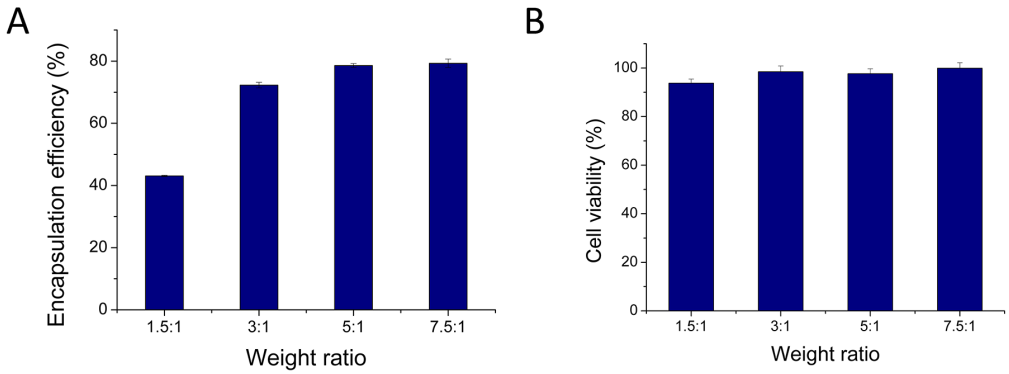

Figure S1. (A) Encapsulation efficiency of FS14-NP for siRNA at different weight ratios of S14 to siRNA, mean ± SD (n=3); (B) Cell viability of FS14-NP/siRNA at indicated weight ratios after 24h. mean ± SD (n=5)

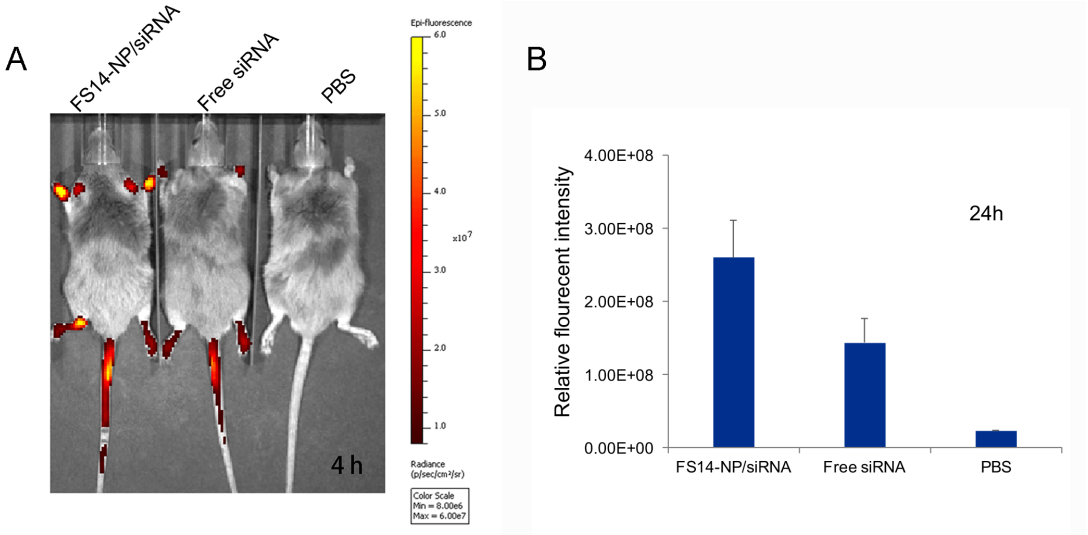

Figure S2. FS14-NP/siRNA accumulation in inflammatory joints. (A) In-vivo imaging showing accumulation of FS14-NP/Cy5.5-siRNA in arthritic joints at 4 h post injection. (B) Quantitative evaluation of the relative fluorescent intensity of the paws after 24 hours. CAIA mice were injected i.v. with FS14-NP/Cy5.5-siRNA (FS14-NP/siRNA), Free Cy5.5-siRNA (Free siRNA) and PBS. The *in vivo* accumulation of FS14-NP/siRNA in arthritic joints was imaged by IVIS at 4 h and 24 h post injection on day 7.

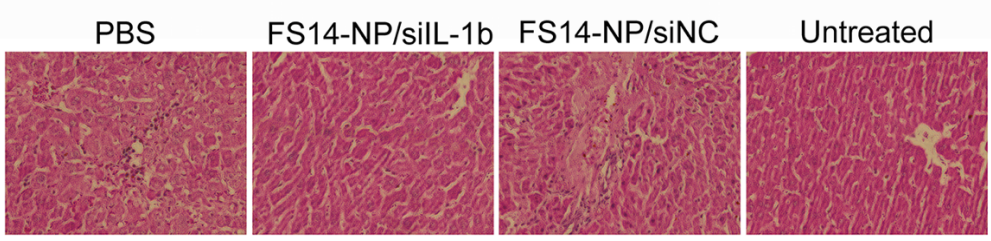

Figure S3. Representative images of H&E staining of liver sections from mice treated with PBS, FS14-NP/siIL-1b, FS14-NP/siNC and comparing to untreated mice.

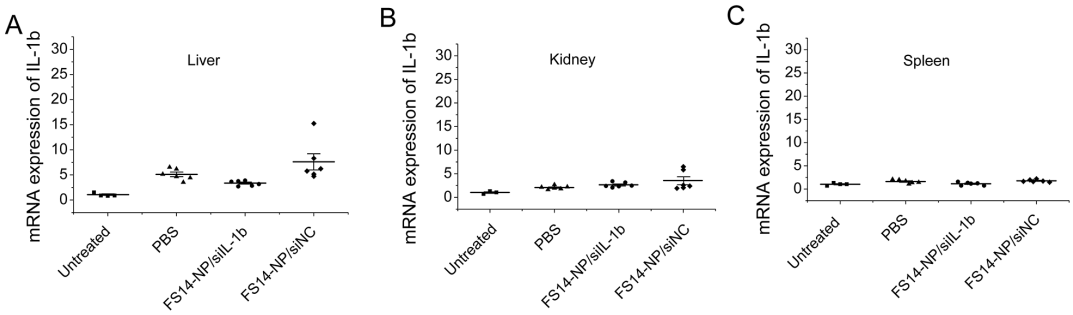

Figure S4. The expression of IL-1β in non-target tissues. Organs were isolated at day 9 and homogenized, the mRNA expression of IL-1β in (A) liver, (B) kidney and (C) spleen were measured by real-time PCR and normalized to housekeeping gene GAPDH.

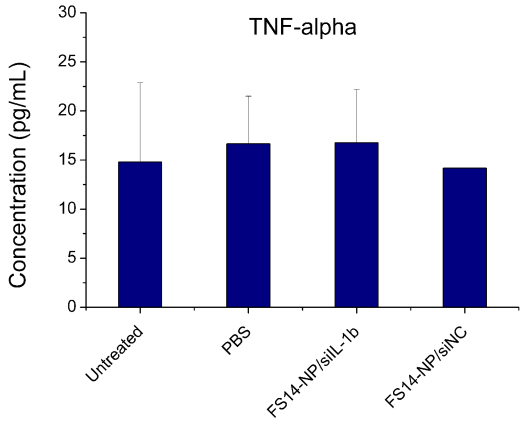

Figure S5. Systemic expression of TNF-α. The expression TNF-α in serum was measured in serum using an Inflammatory Cytokine 4-Plex Mouse Panel kit. Data are presented as mean ± SD (n=6).

Table S1. Primers used for qPCR in the study.

Target (mouse)	Sequence	
IL-1β	F	5′- CAGGCTCCGAGATGAACAAC -3′
	R	5′- GGTGGAGAGCTTTCAGCTCATA -3′
TNF-α	F	5′- GTAGCCCACGTCGTAGGTAA -3′
	R	5′- ATCGGCTGGCACCACTAGTT -3′
MMP-3	F	5′- ATGAAAATGAAGGGTCTTCCGG -3′
	R	5′- GCAGAAGCTCCATACCAGCA -3′
MMP-13	F	5′ - ATGCATTCAGCTATCCTGGCCA -3′
	R	5′ - AAGATTGCATTTCTCGGAGCCTG -3′
GAPDH	F	5′- GACGGCCGCATCTTCTTGTG -3′
	R	5′- GCGCCCAATACGGCCAAATC -3′